

Journal of Materials Chemistry A

Accepted Manuscript



This is an *Accepted Manuscript*, which has been through the Royal Society of Chemistry peer review process and has been accepted for publication.

Accepted Manuscripts are published online shortly after acceptance, before technical editing, formatting and proof reading. Using this free service, authors can make their results available to the community, in citable form, before we publish the edited article. We will replace this *Accepted Manuscript* with the edited and formatted *Advance Article* as soon as it is available.

You can find more information about *Accepted Manuscripts* in the [Information for Authors](#).

Please note that technical editing may introduce minor changes to the text and/or graphics, which may alter content. The journal's standard [Terms & Conditions](#) and the [Ethical guidelines](#) still apply. In no event shall the Royal Society of Chemistry be held responsible for any errors or omissions in this *Accepted Manuscript* or any consequences arising from the use of any information it contains.



Journal Name

ARTICLE

CoO@Co and N-doped mesoporous carbon composite derived from Ionic liquids as cathode catalyst for rechargeable Lithium-oxygen batteries

cReceived 00th January 20xx,
Accepted 00th January 20xx

DOI: 10.1039/x0xx00000x

www.rsc.org/

Wenpeng Ni ^{a, b}, Shimin Liu ^a, Yuqing Fei ^{a, b}, Yude He ^a, Xiangyuan Ma ^a, Liujin Lu ^a and Youquan Deng ^{a,*}

The catalytic activity of a cathode material plays a vital role in determining the electrochemical performance of Li-O₂ batteries. Herein, N-doped mesoporous carbon supported CoO@Co nanoparticles are prepared *in situ* using the ionic liquid (IL) 1-butyl-3-methylimidazolium tetrachlorocobalt ([BMIm]₂[CoCl₄]) as the precursor with silica as the hard template. The material was characterized by TGA, BET, XRD, TEM, XPS, and H₂-TPR. After exposure to air, the species on the surface of the Co is CoO, as verified by XPS. The pore size is about 2 nm, and the CoO@Co nanoparticles were irregularly shaped and sized in the range of 20-300 nm, which may have been due to the aggregation of ultrafine nanoparticles. The existence of an interaction between the CoO@Co nanoparticles and the N-doped support is confirmed by XPS and H₂-TPR. The catalyst shows superior activity for oxygen evolution reaction (OER) manifested in its lower charge potential (3.75 V at the current density of 100 mA g⁻¹). An enhanced performance in coulombic efficiency, rate capability, and cycling stability (55 cycles) are also realized. Finally, these improvements, with the exception of the catalytic activity of CoO, may benefit from the interaction between the carbon supporter and the CoO@Co nanoparticles.

1. Introduction

In recent years, much attention has been paid to non-aqueous lithium-oxygen batteries, which are composed of a lithium anode, an organic electrolyte and a porous cathode, which are exposed to oxygen during cell operation ^[1-6]. The batteries work based on the following reversible reaction, 2Li + O₂ → Li₂O₂. The higher theoretical energy density (about 5200 wh kg⁻¹) of Li-O₂ batteries means they are a promising candidate for applications in electric-vehicles and portable devices. However, in practice, the achievable energy density is much lower than the theoretical value ^[7-10]. Until now, a variety of efforts have been made to overcome the bottlenecks, including the investigating of reaction mechanism ^[11-13],

searching for favourable cathode catalysts and electrolytes ^[14-17], designing the optimum structure of the cathode ^[18-20] and so on. Research that focused on the cathode catalyst achieved impressive results due to the fact that the catalyst was able to lower the activation barriers in the electrochemical reaction steps and reduce the overpotential on discharge and charge. Carbon materials (carbon nanotubes ^[21] and graphene ^[22]), metal oxides (MnO₂ ^[23-25], spinel oxides ^[26] and perovskite oxides ^[27-29]) and nitrides (TiN ^[30] and MoN ^[31]), noble metals and oxides (Pt ^[32], Au ^[33], Pd ^[34], Ru ^[35] and RuO₂ ^[36]) have all been investigated as potential cathode catalysts for Li-O₂ batteries and have shown excellent activity for the oxygen reduction reaction (ORR) and the oxygen evolution reaction (OER). However, the development of more efficient catalysts is still desired for the practical application of Li-O₂ battery.

Cobalt-based oxides, including Co₃O₄, CoO, and cobalt-containing spinels, are considered to be effective cathode catalysts for Li-O₂ batteries ^[37-41]. Co₃O₄ with different morphology ^[42-44] and exposed planes ^[45] has been explored in the recent years. The Co₃O₄ can be mixed with carbon materials to make a cathode according to the method described most frequently in the literatures. It can also be directly deposited onto a nickel substrate ^[43] or a TiO₂ fiber mesh ^[46] to act as a carbon-free cathode. Remarkably, based on the results of a density functional theory (DFT) calculation, among these cobalt-based oxides, CoO showed better catalytic activity and cycling stability due to the favorable adsorption of LiO₂ on the surface of CoO ^[47]. These results have also been verified by different groups, and as such CoO is regarded to be a promising catalyst for Li-O₂ batteries.

Ionic liquids (ILs), which are generally composed of ions based on organic cations and an inorganic anion, have received much attention

^aCentre for Green Chemistry and Catalysis, State Key Laboratory of Solid Lubrication, Lanzhou Institute of Chemical Physics, Chinese Academy of Sciences Lanzhou 730000, China.

^bUniversity of Chinese Academy of Sciences, Beijing 100039, China

Electronic Supplementary Information (ESI) available: TGA curves of [BMIm]Cl and [BMIm]₂[CoCl₄]. The calibration curve for AAS measurement. Nitrogen adsorption-desorption isotherms and the pore size distribution (insert) of XC 72 and C-IL. High resolution Co 2p spectrum of m-CoO@Co/C-IL. High-resolution N 1s spectrum for C-IL and m-CoO@Co/C-IL. Discharge curves at different current density for XC 72 C-IL and CoO@Co/C-IL electrodes. Raman spectroscopy of XC 72 and C-IL. Discharge-charge profiles of cycles for XC 72 and C-IL electrode. High-resolution Co 2p XPS spectrum for electrode before discharge and after discharge. SEM image of C-IL electrode before discharge, after discharge and after charge. See DOI: 10.1039/x0xx00000x

for many years due to their attractive properties such as a large liquidus range, negligible vapor pressure, high ionic conductivity, high thermal stability and a large electrochemical window. Therefore, ILs have been used as green solvents and catalysts in many fields. Additionally, ILs can also be used as a novel type of electrolytes for electrochemical devices such as Li-ion batteries, supercapacitors and Li-O₂ batteries [17]. Furthermore, N-containing ILs are often used as a precursor to prepared N-doped mesoporous carbon materials with or without a template [48]. N-containing cations, such as imidazolium or pyridinium, coupled with dicyanamide (DCA⁻) or bis(trifluoromethylsulfonyl) imide (NTf₂⁻) have been widely studied previously [49-50]. However, cobalt-containing ILs are rarely used to synthesize composites consisting of cobalt-based compounds and N-doped carbon.

In this work, the IL [BMIm]₂[CoCl₄] was used as a precursor to prepared a catalyst for Li-O₂ battery. N-doped mesoporous carbon supported Co nanoparticles were obtained after a calcination process under N₂ atmosphere when a silica template was used. Due to the superior catalytic activity of CoO, the catalyst was exposed to air in order to oxidize the Co to CoO. Amazingly, the charge potential was reduced to 3.75V at a current density of 100 mA g⁻¹ when the catalyst was added to the cathode. The rate capability was also enhanced and the number of cycles increased to 55 when the capacity was limited to the 30% of initial discharge capacity. Based on the results of the contrast experiments, it is postulated that the existence of CoO and the interaction between CoO@Co nanoparticles and N-doped carbon can all be attributed to the improvement in the Li-O₂ battery based on the as-prepared cathode catalyst.

2. Experimental

2.1 Materials synthesis

All the reagents are analytical grade and used without further purification. 1-Methylimidazole and chlorobutane were used as the raw materials to prepared [BMIm]Cl by the method described in a previous report [51], and then the [BMIm]Cl was recrystallized from acetone. For the preparation of [BMIm]₂[CoCl₄], the crystal powder of [BMIm]Cl mixed with CoCl₂·6H₂O at the molar ratio of 2:1 at 80 °C for 5 h [52]. To obtain the silica template, 2 mL of tetraethylorthosilicate (TEOS) was added into a 50 mL mixture containing ethanol and aqueous ammonia (1:2, volume ration) and was kept at 75 °C until the solution evaporated to a powder. The white powder was ground with a mortar and dried at 80 °C in a vacuum dryer.

In the synthesis of the catalyst, 0.5 g of the silica template was mixed with 30 mL ethanol and stirred at 60 °C for 3 h. Then, the solution was poured into [BMIm]₂[CoCl₄] (3 g) and kept it at 80 °C. After the ethanol evaporated, the precursor was transferred to a tubular furnace and calcined at 900 °C for 2 h under N₂ atmosphere. The products were treated in 2 M KOH solution at 80 °C overnight to remove the silica template. After this, the obtained products were washed with deionized water several times and dried at 80 °C in a vacuum dryer. The product is denoted as Co/C-IL, and it was stored in a glove box. The Co/C-IL was exposed to air for at least 10 days to oxidize the Co particles (denoted CoO@Co/C-IL). The same method was used to prepared C-IL when the precursor was

[BMIm]Cl. C-IL was ground together with CoCl₂·6H₂O. Then, the mixture was treated by the same process described above to produce m-CoO@Co/C-IL with the same Co% as CoO@Co/C-IL. For comparison, commercial CoO (99%, Aladdin Industrial Corporation) and Vulcan XC 72 carbon (Cabot) were also used in this work.

2.2 Materials characterization

Thermogravimetric analysis (TGA) was carried out on a Thermogravimetric/Differential Thermal Analyzer (Mettler TGA SDTA851) with a heating rate of 10 °C min⁻¹ from 30 to 800 °C under N₂ flow. X-ray diffraction (XRD) was recorded on a powder XRD system (Siemens D/mas-RB powder X-ray diffractometer) using Cu K α radiation (40 mA and 40 KV). The X-ray photoelectron spectroscopy (XPS) was performed on a VG ESCALAB 210 instrument using Mg K α radiation (1253.6 eV) and the XPS spectra were referred to a C 1s value of 284.6 eV. The morphology was examined by using JEM 2010 high-resolution transmission electron microscopy (HRTEM) operated at 200 keV. Scanning electron microscopy (SEM) analysis was performed with a scanning electron microscope (JEOL-6701F) at an acceleration voltage of 5 kV. Nitrogen adsorption-desorption isotherm measurements were used to investigate the porous structure of the samples with a Micromeritics ASAP 2020 volumetric adsorption analyzer at 76.2 K. Pore size distribution was determined from the adsorption branch of the isotherms based on the density functional theory (DFT). The amount of Co in CoO@Co/C-IL was measured using Atomic Absorption Spectrometry (AAS, Varian AA240). H₂-TPR measurements were taken in a flow system in which H₂-N₂ (5:95) mixed gas was introduced. The water produced by the reduction was trapped on a 4A molecular sieve. The temperature of the sample was programmed to rise at a constant rate of 10 °C/min and the amount of H₂ uptake during the reduction was measured using a thermal conductivity detector and mass spectrometry. Raman spectra were measured with a Thermo Nicolet 5700 FT-Raman accessory spectroscopy meter.

2.3 Electrochemical measurements

The Li-O₂ cell measurements were all carried out at room temperature (about 20±2 °C). A swagelok type cell with an air hole on the cathode side was used to investigate the discharge-charge performance. The cathode was prepared by mixing the as-prepared catalysts (or pure carbon, 90%) and polyvinylidene difluoride (PVDF, 10%) in N-methyl-2-pyrrolidone and then the mixture was coated on a carbon paper disc with a diameter of 20 mm by a scraper and dried at 100 °C for 12 h under vacuum conditions. The typical total loading weight of the cathode material was approximately 1±0.2 mg cm⁻². The Li-O₂ cells were assembled in a glove box with a water and oxygen level of less than 1 ppm. A piece of lithium foil (23 mm in diameter) was used as the anode and was separated by a glass microfiber filter (Whatman GF/D, 25 mm in diameter) with saturated electrolyte. Dimethyl sulfoxide (DMSO) containing 0.1 M LiClO₄ was used as the electrolyte, and the water content was controlled at less than 15 ppm, as verified by Karl Fisher titration. The cell was gas-tight except for the window that exposed the porous cathode film to the oxygen atmosphere. After assembly, the battery was sealed in a glass bottle and purged with a flow of pure O₂ for at least 10 min. The batteries were typically rested for at least 5h before the electrochemical measurements were taken. All

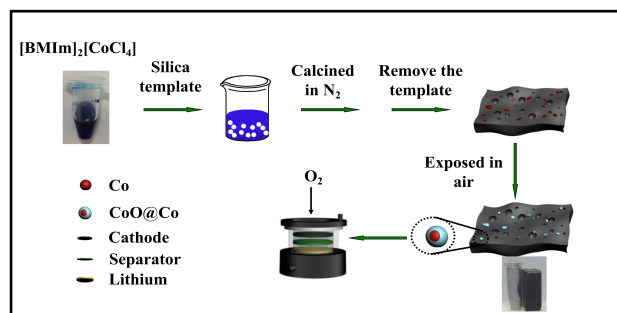


Figure 1. Schematic illustration of the preparation procedure for the CoO@Co/C-IL catalyst and the construction of a Li-O₂ cell.

measurements were conducted under oxygen atmosphere to avoid the negative effects of humidity and CO₂. Galvanostatic discharge-charge measurements were conducted on a LAND battery testing system with the voltage between 2.0-4.2V versus Li/Li⁺ at the current density of 100 mA g⁻¹. The cycling experiments were carried out at a current density of 100 mA g⁻¹ at a depth of 30% of initial capacity. The specific capacity and current density were normalized based on the total mass of catalyst and PVDF in the cathode electrodes. The cyclic voltammetry (CV) and linear sweep voltammetry (LSV) data were collected with a CHI660A electrochemical workstation at a voltage sweep rate of 0.1 mV s⁻¹.

For the SEM and XPS testing of the electrode, the battery was disassembled in the glove box first, and then the cathode was rinsed with acetonitrile (dried by 4A molecular sieve until the water level less than 20 ppm) for several times. The electrode was then dried in vacuum at 70 °C. The electrodes were stored in a sealed bottle, which was placed in the glove box before being transferred to the equipment.

3. Results and discussion

A dark blue colored cobalt-containing IL was used to prepare N-doped carbon supported Co nanoparticles, as shown in Figure 1. After calcining in N₂ and removing the silica template, the Co nanoparticles modifying N-doped mesoporous carbon with magnetic properties were obtained. In order to adjust the catalytic activity of the materials, the sample was exposed to air to transform Co into CoO. Finally, Co nanoparticles coated with CoO and N-doped mesoporous carbon composites were synthesized and used as a cathode catalyst for a Li-O₂ battery.

Firstly, TGA was carried out to gain insight into the thermal decomposition process of the ILs containing silica template, and the results are shown in Figure S1. [BMIm]₂[CoCl₄] was completely carbonized before 650 °C, which is higher than pure [BMIm]Cl (about 320 °C). On the other hand, the weight loss of [BMIm]₂[CoCl₄] (83.5%) was also lower than [BMIm]Cl (96%). In this respect, [BMIm]₂[CoCl₄] is more economical than [BMIm]Cl for use as a precursor to prepared the catalyst. Then, the content of Co in CoO@Co/C-IL was measured by AAS and the result was 35.3% (Figure S2). To further investigate the porosity of the samples, N₂ adsorption-desorption measurements were conducted (Figure 2a). The isotherm was type IV with H₂-shaped hysteresis loops for CoO@Co/C-IL. As shown in the inset of Figure 2a, the pore size

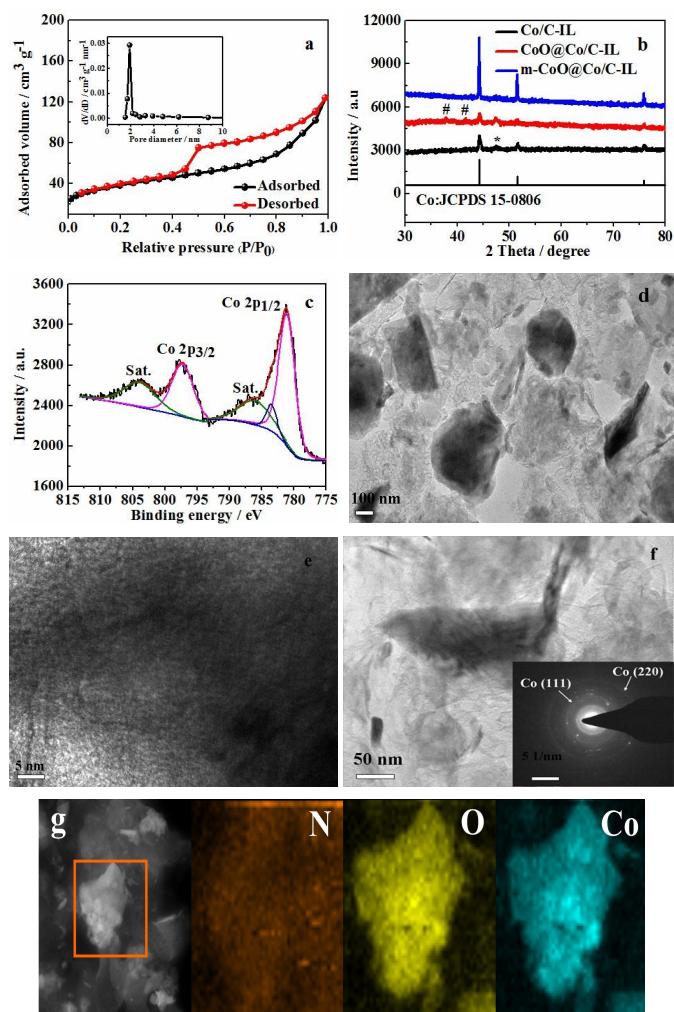


Figure 2. (a) Nitrogen adsorption-desorption isotherms and the pore size distribution (insert) of CoO@Co/C-IL. (b) XRD patterns of Co/C-IL, CoO@Co/C-IL and m-CoO@Co/C-IL. (c) High-resolution Co 2p XPS spectrum for CoO@Co/C-IL. (d) TEM (e) and HRTEM (e) images of CoO@Co/C-IL. (f) SEAD pattern (inset) of CoO@Co/C-IL. (g) EDS mapping of the CoO@Co/C-IL for N, O, and Co elements.

distribution had a major peak at 2 nm calculated from the Barrett-Joyner-Halenda (BJH) method. The calculated specific surface area and pore volume were 139.15 m² g⁻¹ and 0.19 cm³ g⁻¹, respectively. Moreover, the C-IL and XC 72 were also measured and the results are shown in Figure S3a and S3b. The pore size for the two samples was in a wide range of around 2-60 nm. Otherwise, the surface area and pore volume were 58.6 m² g⁻¹ and 0.25 cm³ g⁻¹ for C-IL, respectively, while the result for XC 72 were 251.9 m² g⁻¹ and 0.51 cm³ g⁻¹. The introduction of Co had some influence on the porosity of the materials according to the results of the BET measurements, which were similar to a previous report [53]. It seems reasonable to presume that the well-dispersed CoO@Co nanoparticles would cover some mesopores on the carbon considering the high content of cobalt in this catalyst.

The crystal structure of the samples was characterized by XRD (Figure 2b). The peaks correspond well with the Co phase for the three samples (JCPDS No. 15-0806), while the peak located at

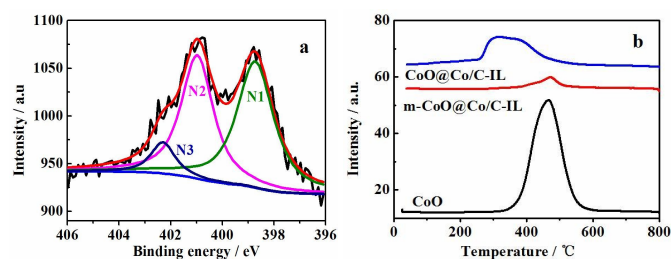


Figure 3 (a) High-resolution N 1s XPS spectrum for CoO@Co/C-IL. (b) H₂-TPR curves of CoO, m-CoO@Co/C-IL and CoO@Co/C-IL.

47.05° can be ascribed to carbon (JCPDS No. 50-1082). In addition, the diffraction peaks of m-CoO@Co/C-IL which have the same amount of Co as CoO@Co/C-IL are stronger and sharper than the two other samples. This could indicate the existence of amorphous structure for Co/C-IL and CoO@Co/C-IL. After exposure to air, the appearance of two minimum diffraction peaks at 36.5 and 42.4° corresponding to the (111) and (200) facets of CoO were observed. Moreover, XPS was used to analyze the species on the surface, and the high-resolution Co 2p XPS spectrum is shown in the Figure 2c. The peak at 781 eV could be assigned to the Co²⁺. In addition, the satellite at about 786 eV is also a characteristic of paramagnetic Co²⁺. These results confirm that the species on the surface of Co nanoparticles is CoO after exposure in air. Moreover, a peak at 782.3 eV was also observed which could be ascribed to the Co-N_x. Furthermore, the surface species of m-CoO@Co/C-IL is also CoO according to the XPS results (Figure S3c). Then, the morphology of the CoO@Co/C-IL was examined by TEM. Figure 2d shows that the CoO@Co particles have irregular shapes and sizes (in the range of 20-300 nm) even though the particles are mostly well-dispersed on the carbon support. However, the HRTEM image (Figure 2e), in which no lattice planes could be observed, revealed that the particles could be the aggregation of ultrafine nanoparticles. The selected area electron diffraction (SEAD) image (Figure 2f) shows the (111) and (220) facets of Co, but they are ambiguous. However, it was difficult to obtain information about CoO. This could be ascribed to the amorphous structure of CoO. EDS mapping was also conducted in order to identify the distribution of the elements (Figure 2g). The results revealed that the N was uniformly distributed in the CoO@Co/C-IL. Additionally, the distribution of O element coincided with that of Co. This means that the O element mainly existed in the form of cobalt oxides in the sample.

It is widely accepted that the catalytic activity of N-doped materials is strongly influenced by the type of nitrogen for the N-doped materials. Therefore, XPS was also performed to explore the properties of N in the samples. For the C-IL (Figure S4a), two distinct peaks were observed in the N1s spectra which could be attributed to pyridinic-type nitrogen (N1, 398.6 eV) and quaternary-type nitrogen (N2, 401.5 eV)^[54]. However, the N3 peak at 402.3 eV was observed except the N1 and N2 peaks for the sample of CoO@Co/C-IL (Figure 3a). This peak is a characteristic of Co-coordinated nitrogen as described in a previous literature^[55]. Furthermore, the binding energy of N2 is 401 eV, which is lower than that of C-IL. These results conclude the existence of the interaction between the CoO@Co nanoparticles and the N-doped

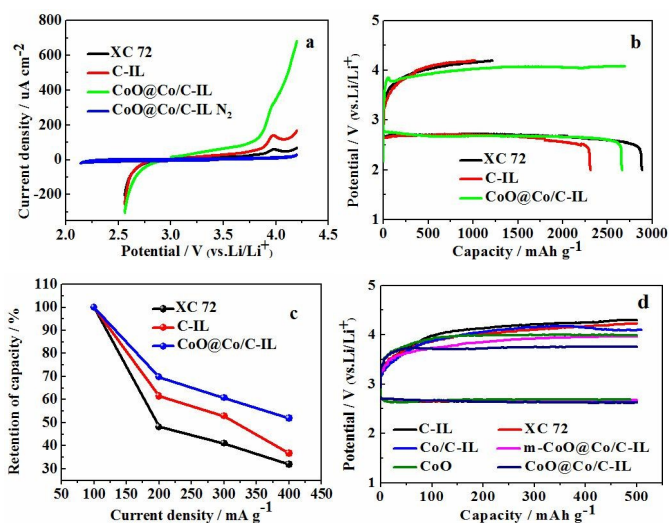


Figure 4 (a) LSV curves of XC 72, C-IL and CoO@Co/C-IL in O₂-saturated DMSO containing 0.1 M LiClO₄. The blue line is the CV of CoO@Co/C-IL in the N₂-saturated electrolyte. (b) The first discharge-charge curves of Li-O₂ batteries with XC 72, C-IL and CoO@Co/C-IL electrodes at 100 mA g⁻¹ in the range of 2.0-4.2 V. (c) Discharge-charge profiles with different materials measured at 100 mA g⁻¹ with a 500 mAh g⁻¹ cutoff specific capacity. (d) The capacity retention capability of Li-O₂ cells with XC 72, C-IL and CoO@Co/C-IL electrodes at various current densities.

carbon, which conform with the analysis of Co 2p. Besides, the N3 peak was not observed for the case of m-CoO@Co/C-IL which was made from a physical mixture of C-IL and cobalt nitrate (Figure S4b). This suggests that CoO@Co and the support prepared *in situ* are essential to the generation of interactions between the two subjects. On the other hand, H₂-TPR has been widely used to study the combined effect of catalysts and supports^[56]. As expected, there are huge differences in the reduced temperature for CoO@Co/C-IL compared to pure CoO and m-CoO@Co/C-IL according to the H₂-TPR curves (Figure 3b). The reduction peak of CoO was centred at 470 °C considering the results of m-CoO@Co/C-IL and pure CoO. Nevertheless, the reduction temperature of CoO@Co/C-IL was in the range of 230-440 °C which is broader and lower than the former two cases. The lower reduction temperature could be attributed to the interaction between CoO@Co and the support which accelerated the reduction of CoO. What is more, the proportion of CoO was about 11.2% and 3.7% for CoO@Co/C-IL and m-CoO@Co/C-IL, respectively, as calculated from the area of the reduction peak when the CuO was used as reference material. As a result, it is reasonable to presume that the interaction has some influences on the properties of the sample which has the potential to affect the catalyst activity for the ORR or OER.

Firstly, the catalytic activity of the sample was studied by LSV firstly. The CV curve of CoO@Co/C-IL shows no obvious redox peak in the N₂-saturated electrolyte which implies the material is stable enough as a cathode catalyst for a Li-O₂ battery (Figure 4a). On the contrary, the ORR and OER peaks appeared in the presence of oxygen for all the three cathodes. Of the three samples, the

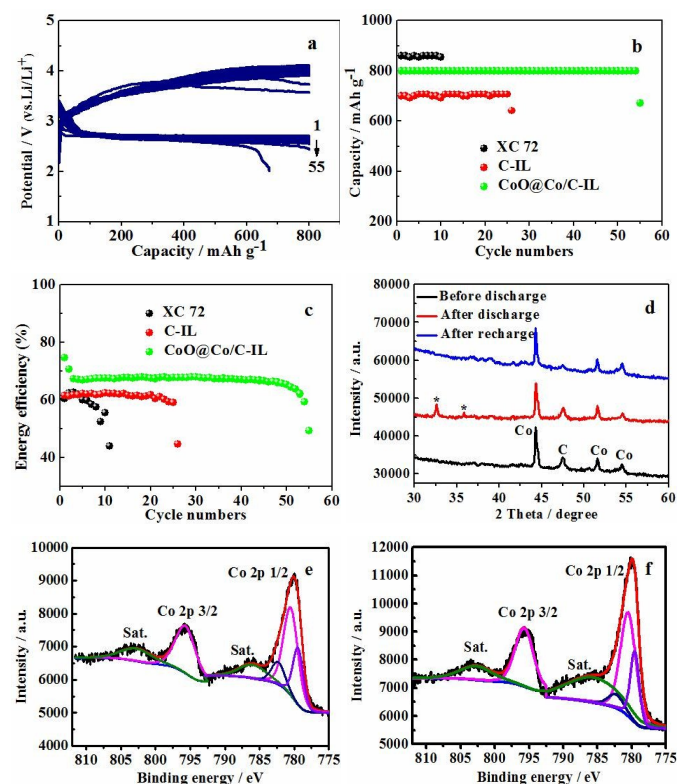


Figure 5. (a) Discharge-charge cycle profiles of cycles with a CoO@Co/C-IL electrode. The variation in discharge capacity (b) and energy efficiency (c) with cycles for XC 72, C-IL and CoO@Co/C-IL electrodes. (d) The XRD patterns of CoO@Co/C-IL at different stages. The high-resolution Co 2p spectrum of CoO@Co/C-IL electrode (e) after recharge, and (f) after 40 cycles.

highest peak current density of the ORR and OER was obtained for the CoO@Co/C-IL among the three samples. Furthermore, the samples have a similar ORR onset potential (about 2.65 V). The OER potential of CoO@Co/C-IL is approximately 3.78 V which is lower than the potential in the other two cases (3.86 V). These improvements indicate the superior activity of CoO@Co/C-IL compared to the pure carbon electrodes. The electrochemical performance was then determined by galvanostatic discharge-charge at a potential range of 2.0 to 4.2 V versus Li/Li⁺ at 100 mA g⁻¹, and the results are illustrated in Figure 4b. The initial discharge capacity of CoO@Co/C-IL, C-IL and XC 72 was 2660, 2310 and 2885 mAh g⁻¹, respectively. The trend in the discharge capacity is consistent with the trend of surface area of the samples. The discharge capacity of CoO@Co/C-IL could be totally recharged while the coulombic efficiency was 42.2% for XC 72 and 44.1% for C-IL. Meanwhile, the charge potential was always lower than 4.0 V for CoO@Co/C-IL which implies a better catalytic activity for OER as compared with the other two materials. The initial discharge capacity was also measured at different current densities to characterize the rate capability of the cells (Figure 4c), and the discharge curves are shown in Figure S5. The capacity only retained 31.9% and 36.7% for XC 72 and C-IL at 400 mA g⁻¹, respectively, while the retention of the capacity for CoO@Co/C-IL was 51.9% under the same

conditions. These results all show the advantages of CoO@Co/C-IL as a cathode materials for Li-O₂ batteries.

In order to explore the nature of the better catalytic activity of the CoO@Co/C-IL, a series of contrast experiments were conducted. As shown in Figure 4d, Li-O₂ batteries with different cathode materials were measured at 100 mA g⁻¹ when the capacity was limited at 500 mAh g⁻¹. The batteries all had the same discharge potential at about 2.64 V while the charge potentials varied greatly. The batteries with pure carbon electrodes (XC 72 and C-IL) possessed the highest charge potential (at 4.3 V and 4.4 V). The charge potential reduced slightly after the electrode was replaced by Co/C-IL which illustrates that Co alone is not effective enough for the OER. Otherwise, due to the superior catalytic activity of CoO, the charge stage is 3.97 V for m-CoO@Co/C-IL and the pure CoO electrode even though the amount of CoO in the former was much less than the pure CoO electrode. This means that the change in the amount of CoO is not the crucial factor in the enhancement of the performance. Nevertheless, the CoO@Co/C-IL had the lowest charge potential at 3.75 V. Besides the catalytic activity of CoO, compared to the m-CoO@Co/C-IL and the CoO electrode, the interaction between the CoO@Co nanoparticles and the N-doped carbon may also play a vital role in the improvement of the performance of the battery. On the other hand, it should be noted that the N-doping did not contribute to the reduction in the charge potential on the basis of the higher charging potential of the C-IL electrode. This result is different from the conclusions of other literatures [57]. In general, a higher catalytic activity of N-doped carbon often shows the formation of structural defects. The defectiveness can be evaluated by Raman spectroscopy. A sample with more defects often shows a higher I_D/I_G ratios. Therefore, the Raman spectroscopy was also conducted for C-IL and XC 72 (Figure S6). The I_D/I_G ratio for XC 72 was 1.05 which is slightly higher than C-IL (0.99). The difference in the I_D/I_G of C-IL and that of other N-doped carbon materials reported by some literatures could interpret the higher charging potential for C-IL.

The cycling stability of the cathode is also an important property for Li-O₂ batteries. The discharge-charge cycle profiles for CoO@Co/C-IL when the capacity was limited at the 30% of initial discharge capacity are shown in Figure 5a. The discharge potential decreased with the increase in cycle numbers while the charge potentials were always lower than 4.0 V until after 47 cycles. For comparison, the cycling stability of the XC 72 and C-IL electrodes were also evaluated, and the discharge-charge profiles are shown in Figure S7. The terminal potentials of the charge process reached 4.5 and 4.4 V for XC 72 and C-IL, which is high enough to induce the side reactions such as the decomposition of electrolyte. As expected, the cycle numbers for the XC 72 and C-IL electrodes were only 11 and 26 while the CoO@Co/C-IL showed a good cyclic performance with negligible decay during 55 cycles as illustrated in Figure 5b. For the CoO@Co/C-IL cathode, the energy efficiency of the first cycle was about 75% which dropped to 67% with the increase in cycle numbers (Figure 5c). However, the energy efficiency was about 60% for XC 72 and C-IL in the first few several cycles. Then, XRD was used to analyze the discharge products of CoO@Co/C-IL (Figure 5d). Except for the diffraction peaks of cobalt and carbon, there are two distinctly diffraction peaks at around 32.7° and 35.2° which can be indexed to the (100) and (101) diffraction of Li₂O₂ after

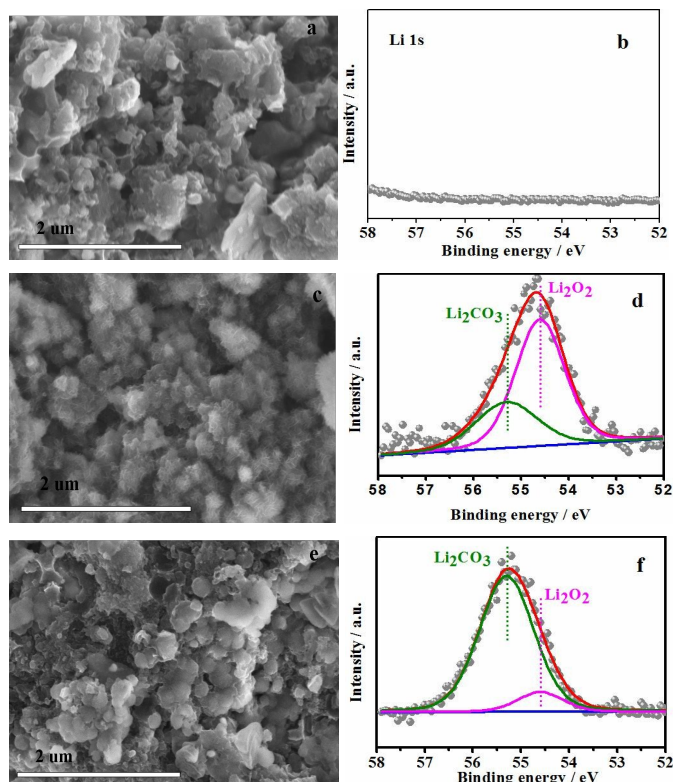


Figure 6. SEM images of CoO@Co/C-IL electrode (a) before discharge, (c) after discharge and (e) after charge. High-resolution Li 1s spectrum of CoO@Co/C-IL electrode (b) before discharge, (d) after discharge and (f) after charge.

discharging. Furthermore, the peaks disappeared after recharging. These results confirm the reversible formation and decomposition of Li_2O_2 . On the other hand, the electrode did not suffer obvious changes in the different stages according to the results of the XRD measurements. However, it is necessary to study the valence change of cobalt by XPS considering the amorphous structure of CoO. Before discharging, the high-resolution Co 2p XPS spectrum of the cathode was similar to that of CoO@Co/C-IL which shows the coexistence of the peaks for Co^{2+} and Co-Nx (Figure S8a). However, the signal corresponding to Co element disappeared after discharging (Figure S8b). This could be attributed to the electrode being covered by discharge products. Furthermore, a new peak at about 779.5 eV which could be ascribed to the Co^{3+} was observed in the spectrum of the electrode after recharging (Figure 5e). This result indicates that the Co^{2+} on the surface was partially oxidized due to the generation of oxidizing species during the operation of the battery. Moreover, the species on the surface of the cathode was the Co^{2+} coupled with Co^{3+} after 40 cycles (Figure 5f).

The variation in the morphology of the electrode at the different stages was also detected by SEM, as shown in Figure 6. Before discharge, the smooth particles were observed, and there was no sign of the Li in the XPS spectrum (Figure 6b). However, the electrode was covered by a layer of products with a flocculent structure after discharging (Figure 6c). The morphology may also play a critical role in reducing the overpotential of charging. It should be noted that the morphology was different from the products on the C-IL

electrode which were submicron toroidal-shaped or sphere particles as for the XC 72 electrode reported by other researchers^[24] (Figure S9b). The XPS results indicated that the discharge products were mainly Li_2O_2 along with some Li_2CO_3 as by-product which may have arisen from a reaction between the Li_2O_2 and the carbon substrate (Figure 6d). In addition, the morphology was recovered after fully recharging. However, the products on the electrode were Li_2CO_3 and some Li_2O_2 as the residues as illustrated in the Figure 6f. The charge potential of CoO@Co/C-IL was much lower than the decomposition voltage of Li_2CO_3 which induces the residual of Li_2CO_3 on the electrode. In one word, the CoO@Co/C-IL was able to effectively catalyze the decomposition of Li_2O_2 .

4. Conclusions

In summary, N-doped mesoporous carbon supported CoO@Co nanoparticles were synthesized from the IL [BMIm]₂[CoCl₄] and employed as a cathode catalyst for Li-O₂ battery. In comparison with the commercial Vulcan XC 72 carbon and C-IL, the as-prepared products exhibited a high catalytic activity towards the OER and the charge potential was 3.75 V at 100 mA g⁻¹. The battery also showed an enhanced rate performance, coulombic efficiency and cycling stability. These improvements could be ascribed to the superior activity of CoO together with the interaction between CoO@Co and the support. Additionally, the flocculent structure of the discharge products also contributed to the reduction in the overpotential. This work sheds some new light on the development of cathode catalysts for high performance Li-O₂ batteries.

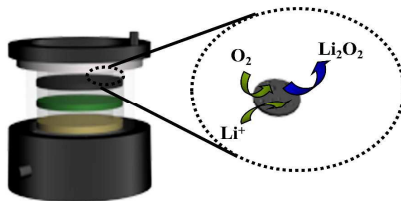
Acknowledgements

This work was financially supported by the National Natural Science Foundation of China (NO. 21403259, 21373247).

Note and references

- 1 K. M. Abraham and Z. Jiang, *J. Electrochem. Soc.*, 1996, **143**, 1-5.
- 2 T. Ogasawara, A. Débart, M. Holzapfel, P. Novak and P. G. Bruce, *J. Am. Chem. Soc.*, 2006, **128**, 1390-1393.
- 3 J. J. Xu, Z. L. Wang, D. Xu, L. L. Zhang and X. B. Zhang, *Nat. Commun.*, 2013, **4**, 2438-2448.
- 4 S. H. Oh, R. Black, E. Pomerantseva, J. H. Lee and L. F. Nazar, *Nature chemistry*, 2012, **4**, 1004-1010.
- 5 R. R. Mitchell, B. M. Gallant, C. V. Thompson and Y. Shao-Horn, *Energy Environ. Sci.*, 2011, **4**, 2952-2958.
- 6 Z. Jian, P. Liu, F. J. Li, P. He, X. W. Guo, M. W. Chen and H. S. Zhou, *Angew. Chem. Int. Ed.*, 2014, **53**, 442-446.
- 7 H. Cheng and K. Scott, *Journal of Power Sources*, 2010, **195**, 1370-1374.
- 8 Y-C. Lu, H. A. Gasteiger, M. C. Parent, V. Chionyan and Y. Shao-Horn, *Electrochemical and Solid-state Letters*, 2010, **13**, A69-A72.
- 9 Y. Chen, F. J. Li, D-M. Tang, Z. L. Jian, C. Liu, D. Golberg, A. Yamada and H. S. Zhou, *J. Mater. Chem. A*, 2013, **1**, 13076-13081.
- 10 J. Gomez, E. E. Kalu, R. Nelson, M. H. Weatherspoon and J. P. Zheng, *J. Mater. Chem. A*, 2013, **1**, 3287-3294.

- 11 D. Y. Zhai, K. C. Lau, H-H Wang, J. G. Wen, D. J. Miller, J. Lu, F. Y. Kang, B. H. Li, W. G. Yang, J. Gao, E. Indacochea, L. A. Curtiss and K. Amine, *Nano Lett.*, 2015, **15**, 1041-1046.
- 12 Z. Q. Peng, Y. H. Chen, P. G. Bruce and Y. Xu, *Angew. Chem. Int. Ed.*, 2015, **54**, 1-5.
- 13 C. Xia, M. Waletzko, L. M. Chen, K. Peppler, P. J. Klar and J. Janek, *ACS Appl. Mater. Interfaces.*, 2014, **6**, 12083-12092.
- 14 W. B. Luo, S. L. Chou, J. Z. Wang, Y. M. Kang, Y. C. Zhai and H. K. Liu, *Chem. Commun.*, 2015, **51**, 8269-8272.
- 15 B. D. Adams, R. Black, Z. Williams, R. Fernandes, M. Cuisinier, E. J. Berg, P. Novak, G. K. Murphy and L. F. Nazar, *Adv. Energy Mater.*, 2015, **5**, 1400867-1400878.
- 16 B. G. Kim, J-N. Lee, D. J. Lee, J-K. Park and J. W. Choi, *ChemsusChem.*, 2013, **6**, 443-448.
- 17 G. A. Elia, J. Hassoun, W. J. Kwak, Y. K. Sun, B. Scrosati, F. Mueller, D. Bresser, S. Passerini, P. Oberhumer, N. Tsiouvaras and J. Reiter, *Nano Lett.*, 2014, **14**, 6572-6577.
- 18 Z. Y. Guo, D. D. Zhou, X. L. Dong, Z. J. Qiu, Y. G. Wang and Y. Y. Xia, *Adv. Mater.*, 2013, **25**, 5668-5672.
- 19 L. J. Cao, F. C. Lv, T. Liu, W. X. Wang, Y. F. Huo, X. Z. Fu, R. Sun and Z. G. Lu, *Chem. Commun.*, 2015, **51**, 4364-4367.
- 20 W. Luo, L. H. Zhou, K. Fu, Z. Yang, J. Y. Wan, M. Manno, Y. G. Yao, H. L. Zhu, B. Yang and L. B. Hu, *Nano Lett.*, 2015, **15**, 6149-6154.
- 21 C. K. Lee and Y. J. Park, *Chem. Commun.*, 2015, **51**, 1210-1213.
- 22 T. Cetinkaya, S. Ozcan, M. Uysal, M. O. Guler and H. Akbulut, *Journal of Power Sources.*, 2014, **267**, 140-147.
- 23 A. Débart, A. J. Paterson, J. L. Bao and P. G. Bruce, *Angew. Chem. Int. Ed.*, 2008, **47**, 4521-4524.
- 24 J. Zhang, Y. P. Luan, Z. Y. Lyu, L. J. Wang, L. L. Xu, K. D. Yuan, F. Pan, M. Lai, Z. L. Liu and W. Chen, *Nanoscale.*, 2015, **7**, 14881-14888.
- 25 A. Zahoor, M. Christy, H. Jang, K. S. Nahm and Y. S. Lee, *Electrochimica Acta.*, 2015, **157**, 299-306.
- 26 S. G. Mohamed, Y-Q. Tsai, C-J. Chen, Y-T. Tsai, T-F. Hung, W-S. Chang and R-S. Liu, *ACS Appl. Mater. Interfaces.*, 2015, **7**, 12038-12046.
- 27 J. J. Xu, Z. L. Wang, D. Xu, F. Z. Meng and X. B. Zhang, *Energy Environ. Sci.*, 2014, **7**, 2213-2219.
- 28 X. P. Han, Y. X. Hu, J. G. Yang, F. Y. Cheng and J. Chen, *Chem. Commun.*, 2014, **50**, 1497-1499.
- 29 W. Yang, J. Salim, S. Li, C. W. Sun, L. Q. Chen, J. B. Goodenough and Y. Kim, *J. Mater. Chem.*, 2012, **22**, 18902-18907.
- 30 F. J. Li, R. Ohnishi, Y. Yamada, J. Kubota, K. Domen, A. Yamada and H. S. Zhou, *Chem. Commun.*, 2013, **49**, 1175-1177.
- 31 S. M. Dong, X. Chen, K. J. Zhang, L. Gu, L. C. Zhang, X. H. Zhou, L. F. Li, Z. H. Liu, P. X. Han, H. X. Xu, J. H. Yao, C. J. Zhang, X. Y. Zhang, C. Q. Shang, G. L. Cui and L. Q. Chen, *Chem. Commun.*, 2011, **47**, 11291-11293.
- 32 J. Y. Cao, S. Y. Liu, J. Xie, S. C. Zhang, G. S. Cao and X. B. Zhao, *ACS Catal.*, 2015, **5**, 241-245.
- 33 W. G. Fan, X. X. Guo, D. D. Xiao and L. Gu, *J. Phys. Chem C.*, 2014, **118**, 7344-7350.
- 34 G. L. Guo, T. H. A. Truong, H. T. Tan, H. X. Ang, W.Y. Zhang, C. Xu, X. H. Rui, Z. L. Hu, E. Fong and Q. Y. Yan, *Chem. Asian J.*, 2014, **9**, 2555-2559.
- 35 B. Sun, P. Munroe and G. X. Wang, *Sci. Rep.*, 2013, **3**, 2247-2253.
- 36 Z. L. Jian, P. Liu, F. J. Li, P. He, X. W. Fuo, M. W. Chen and H. S. Zhou, *Angew. Chem. Int. Ed.*, 2013, **52**, 1-6.
- 37 S. M. Dong, S. Wang, J. Guan, S. M. Li, Z. G. Lan, C. Chen, C. Q. Shang, L. X. Zhang, X. G. Wang, L. Gu, G. L. Cui and L. Q. Chen, *J. Phys. Chem. Lett.*, 2014, **5**, 615-621.
- 38 R. Gao, Z. Y. Li, X. L. Zhang, J. C. Zhang, Z. B. Hu and X. F. Liu, *ACS Catal.*, 2016, **6**, 400-406.
- 39 B. S. Wu, H. Z. Zhang, W. Zhou, M. R. Wang, X. F. Li and H. M. Zhang, *ACS Appl. Mater. Interfaces.*, 2015, **7**, 23182-23189.
- 40 R. Gao, L. Liu, Z. B. Hu, P. Zhang, X. Z. Cao, B. Y. Wang and C. F. Liu, *J. Mater. Chem. A.*, 2015, **3**, 17598-17605.
- 41 B. W. Huang, L. Li, Y. J. He, X. Z. Liao, Y. S. He, W. M. Zhang and Z. F. Ma, *Electrochimica Acta.*, 2014, **137**, 183-189.
- 42 F. Wang, Z. Y. Wen, C. Shen, K. Rui, X. W. Wu and C. H. Chen, *J. Mater. Chem. A.*, 2015, **3**, 7600-7606.
- 43 X. J. Lin, Y. S. Shang, L. Y. Li and A. S. Yu, *ACS Sustainable Chem. Eng.*, 2015, **3**, 903-908.
- 44 D. Oh, J. F. Qi, B. H. Han, G. R. Zhang, T. J. Carney, J. Ohmura, Y. Zhang, Y. Shao-Horn and A. M. Belcher, *Nano Lett.*, 2014, **14**, 4837-4845.
- 45 R. Gao, J. Z. Zhu, X. L. Xiao, Z. B. Hu, J. J. Liu and X. F. Liu, *J. Phys. Chem. C.*, 2015, **119**, 4516-4523.
- 46 S-M. Xu, Q-C. Zhu, F-H. Du, X-H. Li, X. Wei, K-X. Wang and J-S. Chen, *Dalton Trans.*, 2015, **44**, 8678-8684.
- 47 C. Q. Shang, S. M. Dong, P. Hu, J. Guan, D. D. Xiao, X. Chen, L. X. Zhang, L. Gu, G. L. Cui and L. Q. Chen, *Sci. Rep.*, 2015, **5**, 8335-8341.
- 48 S. G. Zhang, M. S. Miran, A. Ikoma, K. Dokko and M. Watanabe, *J. Am. Chem. Soc.*, 2014, **136**, 1690-1693.
- 49 J. S. Lee, X. Q. Wang, H. M. Luo, G. A. Baker and S. Dai, *J. Am. Chem. Soc.*, 2009, **131**, 4596-4597.
- 50 B. J. P. Paraknowitsch, J. Zhang, D. S. Su, A. Thomas and M. Antonietti, *Adv. Mater.*, 2010, **22**, 87-92.
- 51 K. R. Seddon, A. Stark and M-J. Torres, *Pure Appl. Chem.*, 2000, **72**, 2275-2287.
- 52 Q. Wang, Y. R. Geng, X. M. Lu and S. J. Zhang, *ACS Sustainable Chem. Eng.*, 2015, **3**, 340-348.
- 53 Z. L. Li, G. L. Li, L. H. Jiang, J. L. Li, G. Q. Sun, C. G. Xia and F. W. Li, *Angew. Chem. Int. Ed.*, 2015, **54**, 1494-1498.
- 54 W. Grünert, R. Feldhaus, K. Anders, E. S. Shipiro, G. V. Antoshin and K. M. J. Minachev, *J. Electron Spectrosc. Relat. Phenom.*, 1986, **40**, 187-192.
- 55 D. K. Huang, Y. P. Luo, S. H. Li, B. Y. Zhang, Y. Shen and M. K. Wang, *Nano Research.*, 2014, **7**, 1054-1064.
- 56 M. Kang, M. W. Song, C. H. Lee, *Applied Catalysis A: General.*, 2003, **251**, 143-156.
- 57 R. Mi, S. M. Li, X. C. Liu, L. M. Liu, Y. C. Li, J. Mei, Y. G. Chen, H. Liu, H. Wang, H. Yan and W-M. Lau, *J. Mater. Chem. A.*, 2014, **44**, 18746-18753.



N-doped mesoporous carbon supported CoO@Co nanoparticles using ionic liquid as the precursor show superior catalytic activity for Li-O₂ battery.